

Real-time Damping Estimation on Nonlinear Electromechanical Oscillation

Xin Xu, *Student Member, IEEE*, Wenyun Ju, *Member, IEEE*, Bin Wang, *Member, IEEE*, and Kai Sun, *Senior Member, IEEE*

Abstract—Real-time damping estimation for a dominant inter-area mode is important for situational awareness of potential angular instability in power systems. Electromechanical oscillations energized by large disturbances often manifest obvious nonlinearities in measurements on first several swings. Traditional methods based on linear system theory often discard first several swings intentionally to avoid nonlinearity; if not, the estimated damping ratios often vary with the length and starting point of the measuring window. By identifying a nonlinear oscillator to fit a dominant mode, this paper proposes a new measurement-based approach utilizing complete post-disturbance data for robust damping estimation independent of the measuring window. Case studies on the IEEE 9-bus system and a 48-machine Northeast Power Coordinating Council system validate the proposed approach for providing accurate and robust damping estimation compared with the Prony’s method. Meanwhile, three factors influencing damping estimation in practical applications are also addressed, including measurement noises, limited coverage of PMU measurements, and existence of multiple dominant modes.

Index Terms—Damping estimation, nonlinear oscillation, dominant mode, wide area measurement system, WAMS.

I. INTRODUCTION

SUSTAINED inter-area oscillation may potentially lead to angular instability of a power grid. It is important to monitor the dominant inter-area modes for protection and control purposes. In terms of power systems security operation, early recognition of the dominant mode would be beneficial for fast stability and damping assessment and control. Fast and accurate mode identification techniques are always appreciated, especially considering the increasing penetration of the renewable resources which decreases the system inertia and could potentially lead to sustained oscillation [1]-[3]. Those techniques would leave more decision time for the system operators, benefit model parameter estimation [4], and motivate new design of damping controllers. In this paper, the works focus on fast and accurate real-time damping estimation technique, which can be stream-performed, as the first step for new on-line damping controller designs.

Damping ratio is a useful indicator on how critical an oscillation mode is, which can be estimated from the phasor measurement units (PMUs) based wide-area measurement system (WAMS) by modal analysis methods [5]-[7]. Efforts has been reported on the analysis tools for tracking oscillatory dynamics via WAMS [5]. The mainstream methods for measurement-based modal analysis are small-signal analysis methods that are based on linear system and signal theories. They assume the system to be subject to a small disturbance. Thus, a measured system response can be decomposed into exponentially damped/undamped sinusoids with different phases. Henceforth, the main task is to identify eigenvalues and eigenvector-related properties of the targeted modes. One type of methods extracts oscillation modes from ambient measurements caused by random small variations, e.g. in loads. This can be done by reconstructing a linear system from the ambient data while mitigates the impact of the noise, like the autoregressive (AR) type model in [8], whose coefficients are solved by the recursive least square (RLS) type algorithm. Another type of methods, e.g. Prony’s method [9], [10], the Eigenvalue realization algorithm (ERA) [11], and Matrix Pencil method [12], can analyze ring-down measurements following a disturbance such as a line or generator trip. They find the best fitting into the measurements of a window by a sum of sinusoids or by a response from a reconstructed equivalent linear system. Some methods perform time-frequency analysis using the Fourier transform or continuous wavelet transform for better damping estimation [13], [14]. An extended Prony’s method is provided in [14] to extend damping estimation to oscillations under resonance and near-resonance conditions, in which both the dominant modes and the resonances among the modes are considered for more accurate damping estimates.

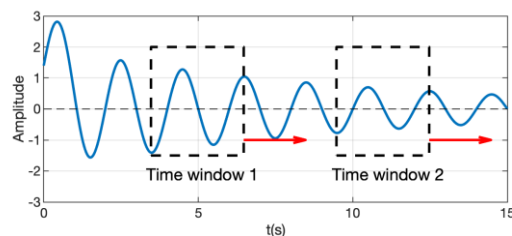


Fig. 1. Schematic diagram of sliding time windows.

This work was supported in part by NSF grants ECCS-1553863 and in part by the ERC Program of the NSF and DOE under grant EEC-1041877.

X. Xu, B. Wang and K. Sun are with the Department of EECS, University of Tennessee, Knoxville, TN 37996 USA (e-mail: xxu30@vols.utk.edu, bwang13@vols.utk.edu, kaisun@utk.edu).

W. Ju is with Electric Power Group, LLC, Pasadena, CA (email: wenyun-ju@gmail.com).

This paper focuses on damping estimation for a dominant inter-area mode using ring-down measurements following a fault. A real-life fault can hardly be treated as a small disturb-

ance especially for areas not too far from the fault location. If the fault excites any critical oscillation mode, nonlinear waveforms often manifest in power system measurements. Thus, in this case, damping estimation using the linear analysis based methods like the Prony's method are often unreliable, since during the early transient stage the results can be sensitive to the length and starting point of the time window as illustrated by Fig. 1. A measure commonly used by many commercialized modal analysis tools is to ignore the first several or several tens of seconds of the ring-down portion containing transient measurements until the system response recovers to be close enough to a linear system response. This handling may discard important information on potential angular instability. Under some conditions, available measurements are too limited, e.g. capturing only first few swings for the critical mode, to afford the discarding of any data. Thus, there is a need for a robust damping estimation tool that is applicable to large-amplitude swings and insensitive to the length and starting point of the measuring window.

Some modal analysis methods have tried to accommodate some nonlinear dynamics. One representative is the Hilbert-Huang transformation (HHT) method [16], in which each mode is interpreted as a sinusoidal signal with time-varying parameters, i.e. a mode with changing frequency and damping. It first extracts so-called intrinsic mode functions (IMF) from measurements by empirical mode decomposition. Each IMF is expected to represent one oscillation mode and interpreted by HHT to estimate time-varying modal parameters. However, these methods are still based on linear system theory and interpret an oscillation mode as a damped/undamped sinusoidal function with time-varying parameters. The resulting damping estimation is still sensitive to the length and starting point of the measuring window.

Theoretically speaking, the nonlinearity in the oscillations is caused by the difference between the original system and the underlying linearized system, which can hardly be ignored under large disturbances. With the same initial value, the response/analytical solution of the original system and the linearized system will be different, and that difference defines the nonlinearity which could be observed in the time-domain measurement data. Alternatively, in terms of the mathematical model, the nonlinearity can be viewed as follows. For an autonomous system ordinary differential equations (ODEs) $\dot{\mathbf{X}} = \mathbf{f}(\mathbf{X})$, $\mathbf{f}(\mathbf{X})$ can be generally approximated by its Taylor's series regarding an operating point. Then, all higher order polynomial terms (order >1) in the series define nonlinearity.

Some recent studies on understanding and formulation of nonlinear electromechanical oscillations discover that the frequency of an oscillation mode decays with the amplitude of oscillation [17], [18] according an "F-A curve". Furthermore, the nonlinear dynamics of a multi-machine system in an extended neighborhood of the equilibrium can be decomposed into dynamics of as many fictitious nonlinear oscillators of 1-DOF (degree of freedom) as its oscillation modes by a Nonlinear Modal Decoupling (NMD) method [19][20]; that is, each decoupled nonlinear oscillator corresponds to a nonlinear mode. Thus, the dynamics and stability of the original system re-

garding each mode can be studied using the corresponding 1-DOF oscillator. For instance, by NMD techniques, it is captured and visualized that when an inter-area 0.6 Hz mode is excited by a large disturbance in the NPCC system, it may evolve into instability without timely remedial control [20].

In this paper, the proposed damping estimation approach inherits the idea of NMD, i.e. each mode could be modeled by a nonlinear oscillator, and fits post-disturbance measurements into a nonlinear oscillator for more robust estimation of oscillation damping, which is less sensitive to the length and starting point of time window of measurements. It is assumed that rotor angles of main generation units can be directly measured or estimated in a real time by PMUs [21]-[23]. [24] also provides an alternative way to estimate the rotor angle by first estimating the rotor speed from the bus voltage phasor speed and then calculate the rotor angle via integral. The approach performs three steps: 1) for approximate modal decomposition, linearly transforming rotor angle measurements into the modal space established from either the linearized system model or online identified from measurements; 2) fitting a nonlinear oscillator for the mode of interest, e.g. the dominant mode; 3) calculating the damping ratio from the oscillator. Also, three factors that could affect the accuracy of damping estimation are introduced, i.e. measurement noises, limited coverage of PMU measurements, and existence of multiple dominant modes, and the corresponding suggestions to reduce their influences and ensure the estimation accuracy are also proposed.

In the rest of the paper, Section II presents the proposed approach. Section III introduces three factors that could affect the accuracy of damping estimation. Section IV tests the proposed approach and compared it with the Prony's method on the IEEE 9-bus system and a 48-machine 140-bus Northeast Power Coordinating Council (NPCC) system. Historical measurement data in the 2011 Southwest Blackout of the Western Electricity Coordinating Council (WECC) system are used to test the feasibility of a purely measurement-based implementation of the proposed approach when the system model is not available. Conclusions are drawn in Section V.

II. NONLINEAR OSCILLATOR FITTING APPROACH

In this section, the three steps of the proposed approach are presented in detail for the damping estimation of a mode of interests like a dominant mode.

A. Modal Decomposition

In this part, a linear transformation matrix is derived to decompose the system response for each mode. Note that the target of the linear transformation is not to perform a perfect modal decomposition, but to roughly extract the response for each mode, especially the dominant modes. The extracted mode response will capture the major dynamic features including the nonlinearity. The extracted mode response may contain some information from other modes due to imperfect decomposition, which can be mitigated by the nonlinear oscillator fitting (NOF) approach as explained later in section II-B.

The linear transformation for decomposing electromechanical modes can be obtained from linearization of the power grid

model in the form of ODEs (1), which can consider detailed generator models with exciters and governors and equivalent impedance loads. The model parameters should be online updated to reflect the current grid topology and system condition.

$$\dot{\mathbf{X}} = \mathbf{f}(\mathbf{X}) \quad (1)$$

where $\mathbf{X} = [\boldsymbol{\delta}, \Delta\boldsymbol{\omega}, \dots]^T$ is a $N \times 1$ vector of system state variables, including rotor angles $\boldsymbol{\delta}$, speed deviations $\Delta\boldsymbol{\omega}$, etc.. \mathbf{f} governs the system dynamics. Note that a power grid model is not available, one may identify an equivalent model from the measurement data by the system identification methods like the Numerical Sub-space State Space System IDentification (N4SID) algorithm [31] that estimates a state-space model capturing the major dynamic features.

Linearize $\mathbf{f}(\mathbf{X})$ at the stable equilibrium (SEP) to obtain

$$\Delta\dot{\mathbf{X}} = \mathbf{A}\Delta\mathbf{X} \quad (2)$$

where \mathbf{A} is the Jacobian matrix.

Let $\Delta\boldsymbol{\delta}$ be the difference between rotor angles $\boldsymbol{\delta}$ and the SEP. The desired linear transformation to decouple dynamics of rotor angles $\Delta\boldsymbol{\delta}$, say \mathbf{T} , is obtained by steps *a*) and *b*) below.

a) Let $\mathbf{A} = \mathbf{L}\boldsymbol{\Lambda}\mathbf{L}^{-1}$, where $\boldsymbol{\Lambda}$ is a diagonal matrix of all eigenvalues and \mathbf{L} is the corresponding modal matrix, whose rows are left eigenvectors. Then, define $\mathbf{Y} = \mathbf{L}\Delta\mathbf{X}$, which includes linearly transformed, decomposed state variables. Amongst $\boldsymbol{\Lambda}$, each conjugate complex pair of eigenvalues, say λ_i and λ_i^* , define one oscillatory mode. If $\lambda_i = \sigma_i + j\omega_i$, the oscillatory frequency $f_{osc,i}$ equals $\omega_i/2\pi$ and damping ratio ζ_i is computed by (3). Assume that N_{osc} modes, i.e. N_{osc} pairs of eigenvalues, have $f_{osc,i}$ in 0.1-2 Hz. They are the modes of electromechanical oscillation (EO) of interests. Re-organize and divide the rows of \mathbf{L} into \mathbf{L}_{osc} and \mathbf{L}_{rest} respectively corresponding to N_{osc} selected EO modes and the other modes as shown in (4).

$$\zeta_i = \frac{-\sigma_i}{\sqrt{\sigma_i^2 + \omega_i^2}} \quad (3)$$

$$\mathbf{Y} = \begin{bmatrix} \mathbf{L}_{osc} \\ \mathbf{L}_{rest} \end{bmatrix} \Delta\mathbf{X} \quad (4)$$

Here, it is assumed that only rotor angles $\boldsymbol{\delta}$ are directly measured by PMUs for online modal analysis. The proposed approach extracts the columns of \mathbf{L}_{osc} that correspond to $\Delta\boldsymbol{\delta}$ to make matrix \mathbf{L}_{osc}^δ . Thus, define

$$\mathbf{Y}_{osc}^\delta = \mathbf{L}_{osc}^\delta \Delta\boldsymbol{\delta} \quad (5)$$

b) Real-valued decomposed state variables are preferred in terms of fitting, but \mathbf{Y}_{osc}^δ is complex-valued due to the complex-valued \mathbf{L}_{osc}^δ . Hence, instead of directly using \mathbf{Y}_{osc}^δ , another transformation \mathbf{P} is adopted [19] to obtain a set of real-valued decomposed state variables, say \mathbf{Z} , as in (6).

$$\mathbf{Z} = \mathbf{P}\mathbf{Y}_{osc}^\delta = \mathbf{P}\mathbf{L}_{osc}^\delta \Delta\boldsymbol{\delta} = \mathbf{T}\Delta\boldsymbol{\delta} \quad (6)$$

$$\begin{cases} \mathbf{Z} = (\mathbf{z}_i)_{N_{osc} \times 1}, \mathbf{z}_i = [\delta_{zi}, \omega_{zi}]^T \\ \mathbf{P} = \text{diag} \left(\begin{bmatrix} 1 & 1 \\ \lambda_i & \lambda_i^* \end{bmatrix} \right) \end{cases} \quad (7)$$

where \mathbf{T} is the desired linear transformation to decouple the dynamics of the oscillation modes from $\Delta\boldsymbol{\delta}$. \mathbf{Z} contains real-valued linearly decomposed state pairs \mathbf{z}_i . Note that $\delta_{zi} = \omega_{zi}$, which makes \mathbf{z}_i behaves like an oscillator, i.e. δ_{zi} behaves like an oscillator ‘‘angle’’ and ω_{zi} behaves like ‘‘speed’’. After de-

composition, each \mathbf{z}_i corresponds to a pair of conjugate complex eigenvalues as indicated by (7), the imaginary part of which tells the oscillation frequency of the mode.

Henceforth, \mathbf{T} is used to decouple the time series measurements of $\Delta\boldsymbol{\delta}$ to obtain a mode of interest, e.g. a dominant mode. One may note that if the SEP cannot be accurately obtained, the time series of $\Delta\boldsymbol{\delta}$ and \mathbf{Z} would contain some constant bias. This will be coped with by the mean centering in Section II-B, and by assuming a fitting model with constant term in Section II-C.

In practical application, as long as any anticipated fault will not significantly change the system model, the transformation \mathbf{T} can be calculated ahead of time, e.g. every 3-5 minutes, or even offline. For accurate estimation, it will be beneficial to keep the model updated as often as possible to reflect the real-time system condition, so that the transformation \mathbf{T} can be the accurate and effective.

B. Nonlinear Oscillator Fitting

Let $\{\mathbf{z}[1], \dots, \mathbf{z}[K]\}$, where $\mathbf{z}[k] = [\delta_z[k], \omega_z[k]]^T$, be the time series of a dominant mode, which oscillates around zero (if not, use techniques like mean centering to meet this requirement [25]). Since each pair \mathbf{z}_i behaves like an oscillator as aforementioned, it is assumed that the time series can be fitted by the nonlinear fitting model (8), which is essentially a nonlinear oscillator of 1-DOF. The high-order polynomial term δ_z^i represents the nonlinearity in the waveform of the dominant mode. Although one may include other nonlinear terms in (8) like the sinusoidal functions, the rationale behind the current model (8) is that an autonomous system having smooth nonlinear functions can generally be approximated by the Taylor expansions of those functions regarding a steady-state condition (i.e. an equilibrium).

$$\ddot{\delta}_z + c_d \dot{\delta}_z + c_1 \delta_z + \sum_{i=2}^L c_i \delta_z^i + c_0 = 0 \quad (8)$$

where c_d and c_i ($i=0, \dots, L$) are the unknowns to be estimated. The constant term c_0 is to allow the existence of constant bias in the time series of $\Delta\boldsymbol{\delta}$ and \mathbf{Z} . L is the highest polynomial order to be selected. A large L can usually give a better fitting since the model (8) has more freedom to accommodate the nonlinearity in system response, and it is recommended to be $L = 30$ based on the experimental results in this paper. $\dot{\delta}_z = \omega_z$, and the time series of $\ddot{\delta}_z$ can be numerically computed via that of $\dot{\delta}_z$, as in [26] and [27]. This oscillator has a stable equilibrium point (SEP), $\delta_{z,SEP}$.

The reason to assume the fitting model (8) is two-folds. First, the Taylor’s expansion of the single machine infinite bus system is in the form of (8), and in NMD, the decoupled 2-dimensional oscillators are also in such form. Second, (8) implicitly allows only one major oscillatory mode component to be identified, and therefore, as long as the noise or information from other modes do not prevail over the target mode, they will be naturally eliminated by implementing the classical least square method as introduced later. Hence, it is preferable to assume the nonlinear oscillator in the form of (8).

Let $\mathbf{C} = [c_d, c_0, \dots, c_L]$, i.e. all the unknowns, $\Psi_k = [\dot{\delta}_z[k], 1, \delta_z[k], (\delta_z[k])^2, \dots, (\delta_z[k])^L]^T$, and $\xi_k = \ddot{\delta}_z[k]$. Then, the estimation

of \mathbf{C} based on least square can be obtained by solving

$$\min_{\mathbf{C}} \text{Obj} = \sum_{k=1}^K (\mathbf{C}\Psi_k + \xi_k)^2 \quad (9)$$

The minimum of (9) is obtained when the derivative vector $\partial \text{Obj} / \partial \mathbf{C}$ is equal to zero, from which the optimal solution \mathbf{C}_{opt} of (9) can be obtained by (10) and (11).

$$\mathbf{C}_{opt} = -\mathbf{v}\mathbf{u}^{-1} \quad (10)$$

$$\mathbf{u} = \sum_{k=1}^K \Psi_k \Psi_k^T, \quad \mathbf{v} = \sum_{k=1}^K \xi_k \Psi_k^T \quad (11)$$

The derivation of (10) and (11) can be found in Appendix A.

C. Calculation of Damping Ratio

Shift the SEP of the oscillator (8) to the origin by replacing δ_z by $\hat{\delta}_z = \delta_z - \delta_{z,SEP}$. The resultant system is represented by (12). Note that all coefficients in (13) are known from Section II-B.

$$\ddot{\hat{\delta}}_z + \hat{c}_d \dot{\hat{\delta}}_z + \hat{c}_1 \hat{\delta}_z + \sum_{i=2}^L \hat{c}_i \hat{\delta}_z^i = 0 \quad (12)$$

The first three terms actually constitute the linear counterpart of (12). The two eigenvalues of the characteristic equation of the linear counterpart can be solved by (13), say λ_{z1} and λ_{z2} . Here, assume $4\hat{c}_1 - \hat{c}_d^2 > 0$ so that λ_{z1} and λ_{z2} are a conjugate pair. The damping ratio ζ_z and the oscillation frequency f_z are calculated by (14).

$$\lambda_{z1}, \lambda_{z2} = \sigma_z \pm jw_z = \frac{-\hat{c}_d}{2} \pm j \frac{\sqrt{4\hat{c}_1 - \hat{c}_d^2}}{2} \quad (13)$$

$$\zeta_z = \frac{-\sigma_z}{\sqrt{\sigma_z^2 + w_z^2}} = \frac{\hat{c}_d}{2\hat{c}_1}, \quad f_z = \frac{w_z}{2\pi} = \frac{\sqrt{4\hat{c}_1 - \hat{c}_d^2}}{4\pi} \quad (14)$$

D. Procedure for Damping Estimation

Using the proposed approach, procedure for estimating the damping ratio of a dominant mode in a real-time, stream-performed manner can be summarized as follows.

Step 1: Transform the measured time series of rotor angles δ within the current sliding time window by (6) to obtain the time series of the linearly transformed, decomposed states \mathbf{Z} .

Step 2: Identify the coefficients of a 1-DOF nonlinear oscillator model (8) on the dominant mode by NOF, i.e. solving (10)-(11).

Step 3: Shift the SEP of the identified oscillator (8) to the origin to obtain (12). The damping ratio can be calculated by (14).

Step 4: Repeat Steps 1-3 for the next time window.

Note that in terms of real-time application, the next time window in Step 4 refers to a period in the future. When the end time instant of the sliding time window is reached, the data of that time period is collected, and Step 1-3 can be implemented automatically with computer programs. The damping estimation process can be finished in real-time since based on section II-A to II-C, the computation part only consists of limited matrix summation and multiplication operations.

For a practical application, the proposed approach can be implemented as an online application based on wide-area measurements from PMUs. The real-time PMU measurements will be fed to the software application of the approach via high-speed communication channels. It is executed continuously on a sliding time window of data to produce the damping

estimation result. The real-time state estimation result is also needed to update the system model and accordingly the modal decomposition matrix \mathbf{T} in order to ensure the accuracy of the steps with equations (4)-(7).

III. INFLUENCING FACTORS ON DAMPING ESTIMATION

In the real-world application, some factors could influence the damping estimation and even worsen the accuracy of the result. In this section, three factors are considered including measurement noises, limited coverage of measurements, and the existence of multiple dominant modes. For each factor, the corresponding suggestions is proposed and illustrated to reduce its impact and ensure the accuracy of damping estimation.

A. Measurement Noises

The noises in measurements can influence estimation accuracy, and thus data preprocessing is needed to screen out the noises in measurements before the estimation. The filter deployed in this paper is similar to the one used in [28], i.e. a low-pass (LP) filter plus a moving average (MA) filter as shown in Fig. 2. In the LP filter, the high frequency noises are extracted by the HP filter, and then, they are removed out of the original measurements by subtraction. MA filter is used to make the filtered data smoother. The proposed approach will be applied to the filtered data afterwards.

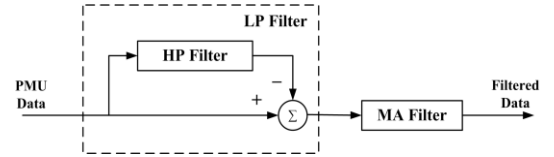


Fig. 2. Schematic diagram of filter for preprocessing measurements.

Compared to an ordinary LP filter, the LP filter in Fig. 2 can keep the low-frequency components less affected than a conventional LP filter when screening out high frequency noises [28]. The requirements for designing the inside HP filter can be found in [29]. The cut-off frequency of the HP filter is recommended to be 2.5Hz in this paper according to the frequency range of electromechanical modes.

B. Limited Coverage of PMU Measurements

For calculating the damping ratio of a dominant mode, the ideal situation is that all rotor angles of generators are available by either direct PMU measurements or dynamic state estimation. However, it could happen that not all rotor angles of generators are measurable by PMUs if either there are no PMUs installed on those generators, or some PMU measurements are not available temporarily due to communication interruption or PMU malfunctions. Thus, the influence of limited coverage of PMU measurements on the accuracy of damping estimation needs to be investigated.

In the case studies of the next section, the impact of missing PMU measurements on the estimation accuracy is investigated by assuming the measurements to be available for down to 85% of generators, e.g. 41 generators for the NPCC system. As later shown in the case studies, if a dominant mode is specified to be monitored during system oscillation, in order to ensure esti-

mation accuracy on oscillation damping, it is recommended to guarantee the accessibility of the PMU measurements of the generators which have high observability of dominant mode.

C. Multiple Dominant Modes

Real-life oscillation events usually involve one dominant mode while the other modes are either insignificant in terms of amplitudes or the impacts on system stability, or do not sustain long. In some specific cases, however, there could be more than one mode that sustain together for a long time before one of them becomes dominant while the rest are damped out, of which the impact on estimation accuracy needs to be studied. Later in the case studies, the scenario with two dominant modes are created and studied on the NPCC 140-bus system, by an excitation technique based on the concept of normal mode [30] which is proposed to specifically excite some modes for power system by initializing the system with linearly scaled mode shape of interest (for short, LSMS): the system is initialized with zero angular velocities and the rotor angles are initialized at the linearly scaled mode shape about the modes of interests.

An index for modal energy is defined to evaluate the modal energy over a sliding time window, such that the energy variation of each mode can be investigated. Similarly define another linear transformation $\mathbf{Y}_{osc}^\omega = \mathbf{L}_{osc}^\omega \Delta \boldsymbol{\omega}$ like in (5). Then, it is real-valued as in (16). Note that the matrix \mathbf{P} here is the same as the one in (7). Thus, \mathbf{z}_i and $\tilde{\mathbf{z}}_i$ correspond to the same pair λ_i and λ_i^* of mode i .

$$\tilde{\mathbf{Z}} = \mathbf{P}\mathbf{Y}_{osc}^\omega = \mathbf{P}\mathbf{L}_{osc}^\omega \Delta \boldsymbol{\omega} = \mathbf{T}_\omega \Delta \boldsymbol{\omega} \quad (15)$$

$$\tilde{\mathbf{Z}} = (\tilde{\mathbf{z}}_i)_{N_{osc} \times 1}, \quad \tilde{\mathbf{z}}_i = [\tilde{\delta}_{z_i}, \tilde{\omega}_{z_i}]^T \quad (16)$$

Then, the index of modal energy E_i of an oscillation mode i can be computed over a sliding time window on the corresponding pair $\tilde{\mathbf{z}}_i$, as (17) and (18). The modal energy ratio (ER) of one mode to the entire modes is defined by (19) to evaluate the dominance of a mode.

$$\tilde{\boldsymbol{\omega}}_{z-i} = \mathbf{T}_{\omega-i}^{-1} \tilde{\mathbf{z}}_i \quad (17)$$

$$E_i = \frac{1}{T_{sl}} \int_{t_0}^{t_0+T_{sl}} \mathbf{H} \tilde{\boldsymbol{\omega}}_{z-i} \quad (18)$$

$$ER_i = \frac{E_i}{\sum E_i} \quad (19)$$

where $\mathbf{T}_{\omega-i}$ contains the columns in \mathbf{T}_ω that correspond to $\tilde{\mathbf{z}}_i$, and the superscript “-1” denotes the pseudoinverse. \mathbf{H} is the row vector of the generator inertia. t_0 is the initial time of the sliding time window, and T_{sl} is the length of the window. A sustained oscillation mode with high amplitude would have a relatively large value of ER_i compared to the fast damped-out or low amplitude modes. Such a mode will be a candidate for a dominant mode to be considered.

IV. CASE STUDIES

In this section, the performance of the proposed approach is first tested on the IEEE 9-bus system and compared with the Prony’s method, eigensystem realization algorithm (ERA), and Hilbert-Huang transform (HHT). Then, it is tested on the NPCC 140-bus system and compared with the Prony’s method to show

its validity on a large system. The measurements are obtained from time-domain simulations under both small and large disturbances. The true value of damping ratio from the linearized model based eigen-analysis is computed by (3) and denoted by “True DR” in the figures. On each test system, a temporary three-phase fault is performed to excite oscillations of the system. The fault is cleared at its critical clearing time (CCT) such that the system response almost loses angular stability and hence has obvious nonlinear transient dynamics.

A WECC event, i.e. the 2011 Southwest Blackout, is used to show a feasible purely measurement-based implementation of the proposed approach when the system model is not available. The computation platform for the case studies is a personal computer with the i7-6700 CPU (3.40GHz) and 16GB RAM. The algorithms for the proposed approach, ERA and HHT are implemented in Matlab, and the Prony’s method is implemented by the Prony tool with the commercial software TSAT by Powertech Labs [7] for online DSA and data-driven oscillation analysis. The TSAT engine and its tools have been integrated into real-time EMS systems in several North-American power companies and interfaced with commercial phasor data concentrators (PDCs).

A. IEEE 9-bus System

The model of IEEE 9-bus system is from [21], with the classical generator model and constant impedance load considered. The system data are given in Fig. 3. A temporary three-phase fault is added at bus 5 and cleared at the critical clearing time (CCT) with the line 5-7 being disconnected. The sampling rate is 30 samples per second.

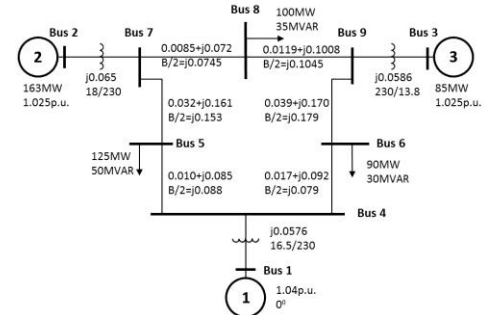


Fig. 3. Schematic diagram of the IEEE 9-bus system [21].

The 0.97 Hz oscillation mode is largely excited and hence selected for damping estimation. The dominance of the 0.97 Hz mode can also be verified by the spectrums from the response of two relative rotor angle differences, as shown in Fig. 4. The information related to this dominant mode from linearized model based small signal analysis is given in TABLE I.

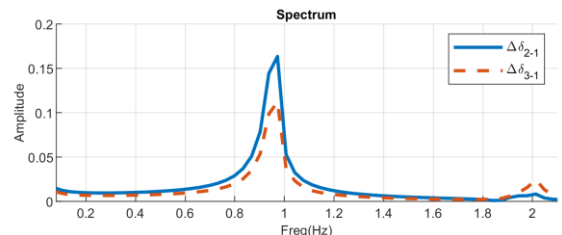


Fig. 4. IEEE 9-bus system: spectrums when the fault cleared at CCT.

TABLE I. DOMINANT MODE INFO

Frequency (Hz)	Eigenvalue	Damping ratio (%)
0.97	-0.100 - 6.089i	1.642

Different lengths of sliding time windows are selected, i.e. 2 s, 2.5 s, 3 s, 3.5 s, 4 s. Order $L = 10$ is selected to fit the model in (8) since its result is close to that of $L = 30$. The results are compared with the results from the Prony's method, ERA and HHT on the response of $\Delta\delta_{2-1}$ as shown in Fig. 5, which validates the proposed approach for providing accurate and robust damping estimation. Note that the initial time instant of each sliding time window is used as the timestamp for the corresponding estimation. The damping ratio of the dominant mode estimated from the proposed approach is much less sensitive to the length of the sliding time window, which indicates the true damping of the mode in the sense of both small and large disturbances. Hence, compared with the other methods, the proposed approach is more reliable for the first several large-amplitude swings following the large disturbance. Moreover, it has a high accuracy even with short time windows. Thus, the proposed approach has obvious advantages for real-time applications.

In addition, here \mathbf{T} is calculated from the pre-fault system model while the mode identification is on the response of the post-fault system. The result shows the robustness of the proposed method against moderate changes of the system model like non-extreme faults.

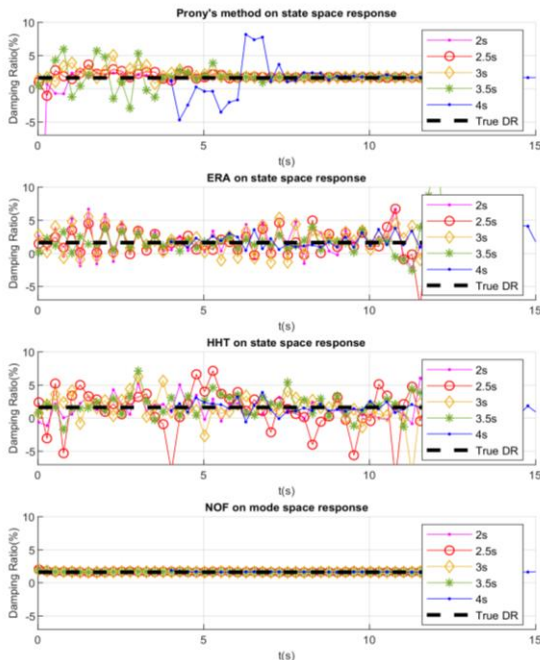


Fig. 5. Comparison on the IEEE 9-bus system: Prony's method, ERA and HHT on the state space response $\Delta\delta_{2-1}$ and NOF on mode space response.

Below, a more fair comparison study is conducted to verify whether the improvement in damping estimation is only because of modal decomposition \mathbf{T} or not and the necessity of NOF to deal with nonlinearity in oscillation. Specifically, the Prony's method, ERA and HHT are also implemented on mode-decomposed time series of the dominant mode, which are

generated by the same steps (4)-(7) as those with NOF. The results in shown in Fig. 6. Compared with Fig. 5, although the damping estimates by the three linear methods are improved, they are still not as accurate as the proposed approach, and their results are sensitive to the selection of the window length.

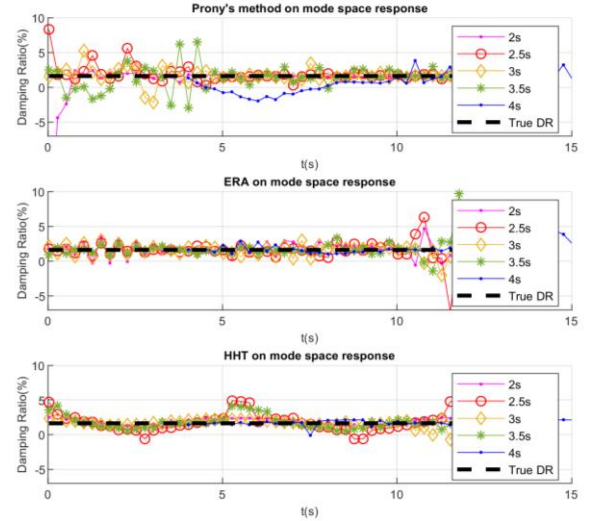


Fig. 6. Comparison on the IEEE 9-bus system: Prony's method, ERA and HHT on the mode space response.

B. NPCC 140-bus System

The NPCC system has 27 of 48 generators modeled by detailed 4th order generator models with exciters [32] and is used as a more realistic grid model to demonstrate the validity of the proposed approach. The system one-line diagram is given in Fig. 7. A large, temporary three-phase fault is added at bus 13 and cleared after a duration of (a) CCT, (b) 0.5 CCT, and (c) 0.25 CCT, respectively, without disconnecting any line. An oscillation mode at around 0.60 Hz is selected for damping estimation, which is a critical inter-area mode that causes two groups of generators swinging against each other as shown in Fig. 7. The partition of the two groups is determined from the mode shape [20]. The simulation results are recorded in 30 samples per second, the same as a typical PMU sampling rate.

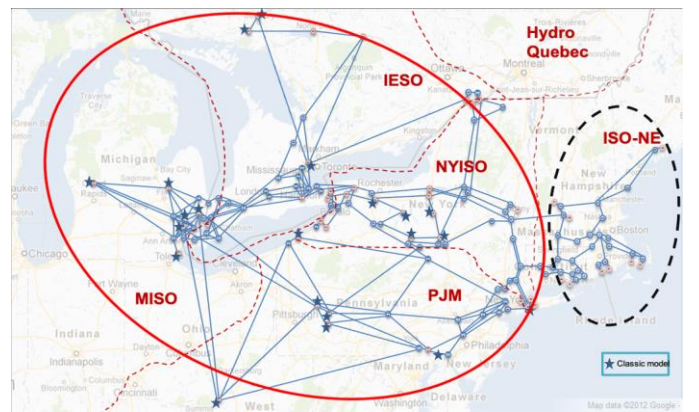


Fig. 7. One-line diagram of the NPCC 140-bus power system and the two groups that swing against each other under the 0.60 Hz mode [20].

The dominance of the 0.60 Hz mode can also be verified by the spectrums from the responses of five rotor angles relative to generator 1, as in Fig. 8. The information related to this dominant mode from linearized model based small signal analysis is

given in TABLE II.

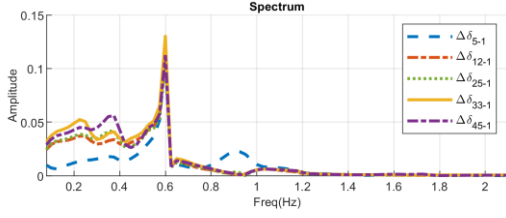


Fig. 8. NPCC 140-bus system: Spectrums when the fault is cleared at CCT.

TABLE II. DOMINANT MODE INFO

Frequency (Hz)	Eigenvalue	Damping ratio (%)
0.60	$-0.037 \pm 3.807i$	0.983

Different lengths of the sliding time window as 3 s, 3.5 s, 4 s, 4.5 s, and 5 s are selected. $L=30$ is selected to fit the model in (8). The Prony’s method is performed on the rotor angle difference between generators 29 and 5, since the 0.60Hz mode is highly observable from the measurements of δ_{29} and δ_5 , and δ_{29} and δ_5 are nearly out-of-phase. The results with fault durations of (a) CCT, (b) 0.5 CCT, and (c) 0.25 CCT are shown in Fig. 9, Fig. 10, and Fig. 11, respectively. The proposed approach is much more robust than the Prony’s method. Moreover, the proposed approach can give more consistent damping estimation regardless of the length of the sliding time window. Therefore, the proposed approach can also be applied to a large power system if its model is provided.

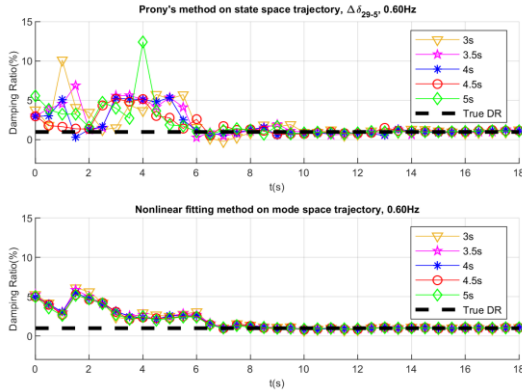


Fig. 9. Comparison on the NPCC system with a fault cleared at CCT.

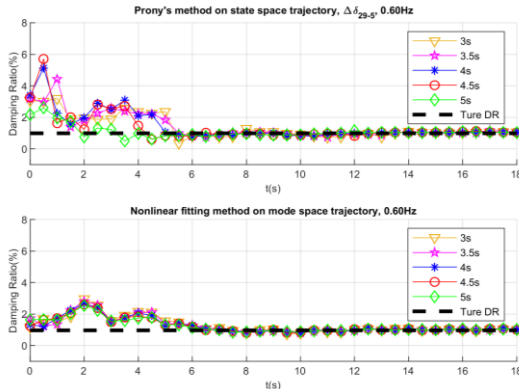


Fig. 10. Comparison on the NPCC system with a fault cleared at 0.5×CCT.

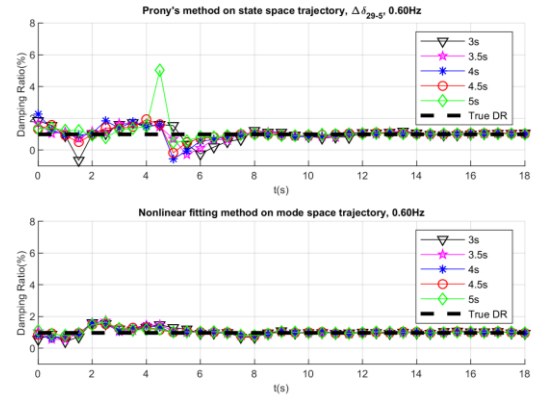


Fig. 11. Comparison on the NPCC system with a fault cleared at 0.25×CCT.

Note that when the fault is cleared at CCT, the system nonlinearity is significantly excited and the result of the proposed approach in Fig. 9 deviates away from the true damping ratio during the first 7 seconds. This phenomenon indicates that the proposed approach can obtain the “True DR” with the system nonlinearity manifested up to some extent. Therefore, there exists an accuracy region for the proposed approach in the state space, within which the proposed approach can provide a high-accuracy estimation. However, investigating the accuracy region is difficult and computationally intensive due to the high-dimensionality nature of the original state space. Instead, an indicator is defined in this paper to evaluate how close the estimation result is to the “True DR”.

The experimental result shows that, when the estimation from the proposed approach is not close to the ‘True DR’, the coefficient of the 4th order term, c_4 in (9), is usually ten times larger than the coefficient of the 3rd order terms, c_3 ; otherwise, c_4 usually stays small. This indicates that the proposed approach might encounter considerable errors when the 4th or higher order monomials become unneglectable. Moreover, the post-fault trajectory shows more nonlinearity when the initial value is close to the stability boundary. Hence, an indicator is defined as (20) via the rotor angles and the type-1 UEP (unstable equilibrium point) whose unstable manifold would be intersected by the fault-on trajectory if the fault sustains. The type-1 controlling UEP is used since it characterizes the portion of the stability boundary near the fault-on trajectory [33]. It could be obtained by using the BCU method [34]. For the sake of convenience, in this paper, it is alternatively approximated by the point in the first swing of the post-fault trajectory where the generators have the least rotor speed difference, since at the UEP the rotor speed difference among the generators should be zero.

$$Ind = \left\| \frac{\Delta\delta}{d_{uep}} \right\|^4 \quad (20)$$

where d_{uep} is the distance between the type-1 UEP and SEP; $\| \cdot \|$ is the operator to solve the 2-norm.

When Ind is smaller than a certain threshold, the nonlinearity caused by 4th and higher order terms are considered ignorable or limited. Based on the experimental results, it is suggested to set the threshold of Ind as 0.02, or equivalently $\| \Delta\delta/d_{uep} \| <$

0.376, to obtain a good estimation of the accuracy region of the proposed approach. As shown in Fig. 12, the variation of $\|\Delta\delta/d_{\text{uep}}\|$ is less than the threshold 0.376 after 7 seconds, after which the estimation become more close to the ‘‘True DR’’ as shown in Fig. 9.

To investigate the phenomenon that the estimated damping ratio deviates from the ‘True DR’ during the first 7 seconds in Fig. 9, i.e. CCT case, the mode ‘angle’ $\Delta\delta_{zi}$ of the 0.60 Hz mode is investigated, of which the time series is shown in Fig. 13. The two envelopes (in red) of the time series (in blue) tend to converge in a fast pace before the 7 seconds, while in a low pace afterwards. This shows that the 0.60 Hz mode undergoes a fast damped out process during the early transient stage where system nonlinearity is largely excited. This property could motivate a new type of stabilization control methods which not only consider the linear system responses, but also consider the nonlinear system responses to some extent.

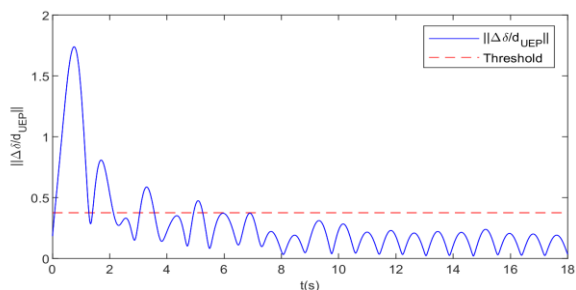


Fig. 12. Variation of $\|\Delta\delta/d_{\text{uep}}\|$.

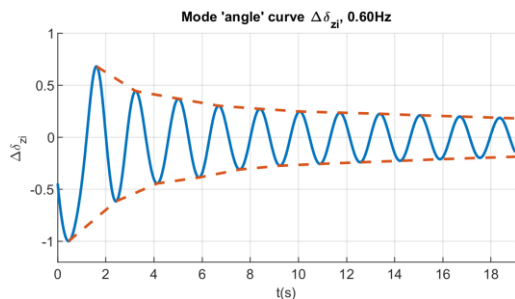


Fig. 13. Mode ‘angle’ curve $\Delta\delta_{zi}$ of the 0.60 Hz mode.

C. Studying Three Influencing Factors on the NPCC system

Influences of three factors mentioned in Section III on damping estimation are investigated here on the NPCC 140-bus system.

1) Measurement Noises

Assume that the time series of rotor angle δ from the case in Section IV-B contain a Gaussian noise with a variance of 0.005. Without screening out the noise, the proposed approach even cannot give an acceptable result. Then, the filter in Fig. 2 is applied to screen out the noise, and the proposed approach is applied to the filtered time series of rotor angles over a 5 seconds sliding time window. The estimation result is compared with that of ‘‘No noise’’ scenario, as illustrated in Fig. 14. The comparison shows that with the designed filter, the damping estimation result is close to that with no noise.

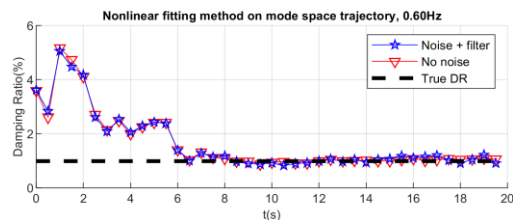


Fig. 14. Damping ratio estimation with noise in time series.

2) Limited Coverage of PMU Measurements

The limited coverage of PMU measurements could influence the accuracy of damping estimation. Moreover, if the unavailable PMU measurements are from those generators with high observability of the dominant mode, it could have more severe influence on the accuracy of damping estimation. For the NPCC system, the 0.60 Hz mode is highly observable from generators 5, 28, and 29 based on their mode shapes. The accessibility of their PMU measurements is of great interests.

Consider three scenarios:

Scenario 1: the PMU measurements from 41 generators are available (85% coverage), and the PMU measurements for generators 5, 28 and 29 are not available;

Scenario 2: the PMU measurements from 41 generators are available, (85% coverage), and the PMU measurements for generators 5, 28 and 29 are available;

Scenario 3: the PMU measurements for all the 48 generators are available (100% coverage).

The estimation results for the above three scenarios are compared in Fig. 15.

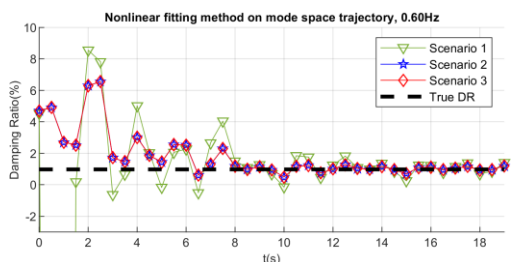


Fig. 15. Damping ratio estimation with limited PMU coverage.

The results in Fig. 15 shows that, if the measurements on those generators with high observability of the dominant mode are not available, the estimation accuracy will be worsen, as the comparison between **Scenario 1** and **Scenario 3**; otherwise, the estimation result would still remain accurate, as the comparison between **Scenario 2** and **Scenario 3**. Therefore, if a dominant mode is specified to be monitored during system oscillation, it is strongly recommended to guarantee the accessibility of PMU measurements on the generators which have high observability of that dominant mode in order to ensure the accuracy of damping estimation.

The above comparison shows the importance of PMU placement on the system observability and estimation accuracy. According to [35], high observability to power system dynamics under large disturbances can be achieved by optimal PMU placement via empirical observability Gramian. It shows that with the optimization method in [35], dynamic state estimation for the same NPCC system can be fairly accurate when

PMUs are installed on only a small percentage (e.g. 25-30%) of buses which are optimally determined.

3) Scenario with Two Dominant Modes

In this subsection, a scenario with two dominant modes, the 0.46 Hz and 0.60 Hz modes, co-existing are studied. The two modes are intentionally excited using the LSMS technique introduced in Section III-C. The response of the relative rotor angles is given in Fig. 16. The proposed approach is applied using a 5 seconds sliding time window. The modal energy ratio, i.e. ER defined in (19), are calculated for both modes.

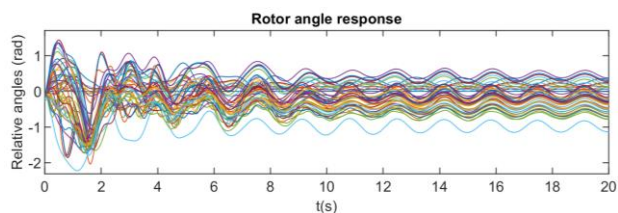


Fig. 16. Rotor angle response.

The variation in measured damping ratios and the variation in modal energy ratios are shown in Fig. 17 for the two modes. During the early transient period of the first few seconds, the 0.46 Hz mode is more dominant since it has the highest energy ratio among all oscillation modes. The damping ratio estimation is more accurate for the 0.46 Hz mode than for the 0.60 Hz mode. Then, at 5.6 seconds, the 0.60 Hz mode raises its modal energy ratio to be the same as the 0.46 Hz mode, and then becomes more dominant. Thereafter, the damping ratio of the 0.60 Hz mode becomes more accurate while the 0.46 Hz is quickly damped with its modal energy ratio decreasing to <10% after $t = 11$ s, at which its damping estimation is terminated as in Fig. 17.

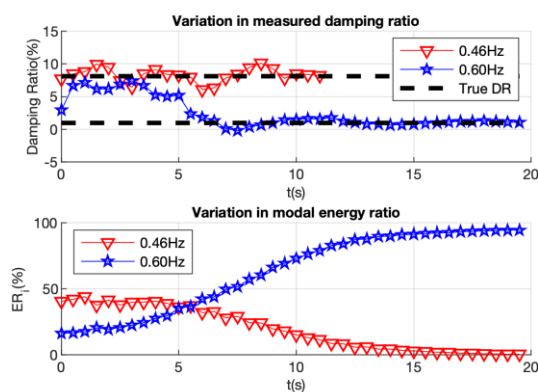


Fig. 17. Variation in measured damping ratio and variation in modal energy ratio (ER).

From the analysis above, it shows that the proposed approach can give more accurate damping estimation for a more dominant mode in terms of the defined modal energy ratio, which could be used to determine the most dominant mode in online applications and as an indicator on if the damping estimation using the proposed approach is accurate. The energy ratio could also be utilized for designing transient stability analysis and control methods.

D. WECC Event

The 2011 Southwest Blackout event was caused by cascading failures. As shown in Fig. 18, the historical data of forty seconds from ten PMUs are used to test the proposed approach in a practical condition when the system model is not available. An equivalent system model is obtained by applying the N4SID algorithm to the portion of data without big oscillations, between 22:38:00 and 22:38:12. The data with big oscillation, between 22:38:23 and 22:38:31, are used for damping estimation, and a mode of around 0.4 Hz is selected to be monitored. The result from the proposed approach is shown in Fig. 19. Note that between 22:38:27 and 22:38:30, the measured damping ratio decreases to a negative value, and then, becomes positive again, which was caused by several generator trips as verified by [36]. Therefore, this example demonstrates the feasibility of a purely measurement-based implementation of the proposed method by means of a data-driven equivalent model, and the estimation result could be helpful for monitoring damping information with a dominant mode.

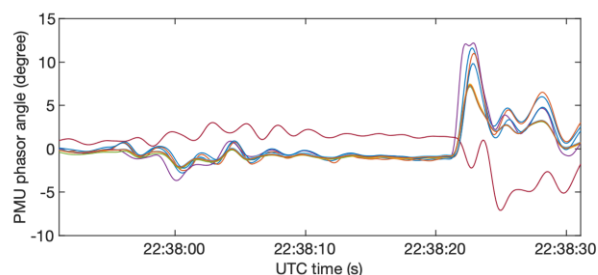


Fig. 18. PMU measurement of 2011 Southwest Blackout.

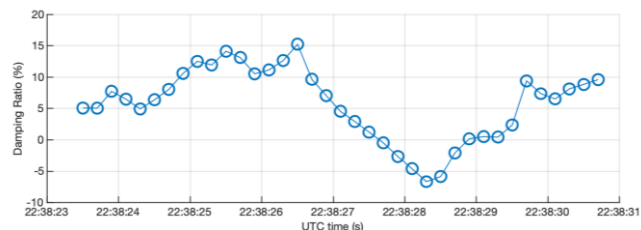


Fig. 19. Estimated damping ratio for Southwest Blackout.

V. CONCLUSIONS

A new approach is proposed for accurate real-time damping estimation on power system oscillation energized by either small or large disturbances. Compared with the conventional Prony's method or other methods with linear system response assumption, the proposed approach is based on the fitting of a nonlinear oscillator regarding a mode of interest and it discovers the meaning of damping under both small and large disturbances. Test results demonstrated that damping ratios estimated by this new approach are more consistent under large disturbances and less sensitive to the selected length of the sliding time window for estimation. Future work includes how to modify the modal decomposition to better cope with the strong nonlinearity in the system response, how to estimate damping ratios of multiple dominant modes, the implementation issues with realistic wide-area measurements, and the application of the proposed approach for damping control.

APPENDIX A

The global optimal solution to reach the minimum of the least square problem (9) must satisfy a necessary condition as shown by (21).

$$\frac{\partial Obj}{\partial \mathbf{C}} = \left[\frac{dObj}{dC_1} \quad \frac{dObj}{dC_2} \quad \dots \right] = 0 \quad (21)$$

Note that C_i denotes the i th entry in $\mathbf{C} = [c_d, c_0, \dots, c_L]$. Each entry in (21) is calculated by

$$\frac{dObj}{dC_i} = 2 \sum_{k=1}^K \Psi_{k,i} (\mathbf{C}\Psi_k + \xi_k) \quad (22)$$

where $\Psi_{k,i}$ is the i th entry in Ψ_k .

Since $(\mathbf{C}\Psi_k + \xi_k)$ is a scalar, (21) can be rewritten as a compact form as (23) by substituting (22) into (21).

$$\frac{\partial Obj}{\partial \mathbf{C}} = 2 \left(\mathbf{C} \sum_{k=1}^K \Psi_k \Psi_k^T + \sum_{k=1}^K \xi_k \Psi_k^T \right) = 2(\mathbf{C}\mathbf{u} + \mathbf{v}) = 0 \quad (23)$$

where \mathbf{u} and \mathbf{v} are defined in (11). Since (23) has a unique solution, i.e. (24), it is also the global optimal solution that can reach the minimum of (9).

$$\mathbf{C}_{opt} = -\mathbf{v}\mathbf{u}^{-1} \quad (24)$$

REFERENCES

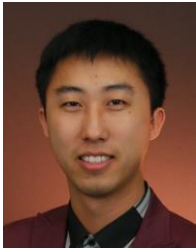
- [1] J. Pierre, et al, Identification of Electromechanical Modes in Power Systems, IEEE Task Force Rep., Jun. 2012, Special Publication TP462.
- [2] J. Quintero, et al, "The Impact of Increased Penetration of Converter Control-Based Generators on Power System Modes of Oscillation," *IEEE Trans. Power Syst.*, vol. 29, no. 5, pp. 2248-2256, Sept. 2014.
- [3] Y. Liu, S. You, J. Tan, Y. Zhang and Y. Liu, "Frequency Response Assessment and Enhancement of the U.S. Power Grids Toward Extra-High Photovoltaic Generation Penetrations—An Industry Perspective," *IEEE Trans. Power Syst.*, vol. 33, no. 3, pp. 3438-3449, May 2018.
- [4] G. Song, S. Norris, J. Bialek. "Adaptive parameter estimation of power system dynamic model using modal information." *IEEE Trans. Power Syst.*, vol. 29, no. 6, pp. 2854-2861, Nov. 2014.
- [5] J. F. Hauer, D. J. Trudnowski and J. G. DeSteese, "A Perspective on WAMS Analysis Tools for Tracking of Oscillatory Dynamics," *IEEE PES General Meeting*, Tampa, FL, 2007.
- [6] Jianzhong Tong and Lei Wang, "Design of a DSA Tool for Real Time System Operations", *PowerCon*, Chongqing, China, Oct. 2006.
- [7] L. Wang, "Techniques for high performance analysis of transient stability," *IEEE PES General Meeting*, San Diego, CA, 2012.
- [8] N. Zhou, J. W. Pierre, D. J. Trudnowski, R. T. Guttromson, "Robust RLS methods for online estimation of power system electromechanical modes," *IEEE Trans. Power Syst.*, vol. 22, no. 3, pp. 1240-1249, Aug. 2007.
- [9] J. Hauer, et al, "Initial results in Prony analysis of power system response signals," *IEEE Trans. Power Syst.*, vol. 5, no. 1, pp. 80-89, Feb. 1990.
- [10] J. F. Hauer, "Application of prony analysis to the determination of modal content and equivalent models for measured power system response," *IEEE Trans. Power Syst.*, vol. 6, no. 3, pp. 1062-1068, Aug. 1991.
- [11] J. N. Juang, R. S. Pappa, "An eigensystem realization algorithm for modal parameter identification and model reduction," *J. Guidance, Control, Dynam.*, vol. 8, no. 5, pp. 620-627, Sep. 1985.
- [12] Y. Hua, T. K. Sarkar, "Matrix pencil method for estimating parameters of exponentially damped/undamped sinusoids in noise," *IEEE Trans. Acoust., Speech, Signal Process.*, vol. 38, no. 5, pp. 814-824, May 1990.
- [13] K. Poon, K. Lee, "Analysis of transient swings in large interconnected power systems by Fourier transformation," *IEEE Trans. Power Syst.*, vol. 3, no. 4, pp. 1573-1579, Nov. 1988.
- [14] J. L. Rueda, C. A. Juarez, I. Erlich, "Wavelet-based analysis of power system low-frequency electromechanical oscillations," *IEEE Trans. Power Syst.*, vol. 26, pp. 1733-1743, 2011.
- [15] T. Xia, Z. Yu, K. Sun, D. Shi, Z. Wang, "Extended Prony Analysis on Power System Oscillation under a Near-Resonance Condition," *IEEE PES General Meeting*, 2020.
- [16] N. E. Huang, et al, "The empirical mode decomposition and the Hilbert spectrum for nonlinear and nonstationary time series analysis," *Proc. R. Soc. London*, vol. 454, pp. 903-995, 1998.
- [17] B. Wang, K. Sun, "Formulation and characterization of power system electromechanical oscillations," *IEEE Trans. Power Syst.*, vol. 31, no. 6, pp. 5082-5093, Nov. 2016.
- [18] B. Wang, X. Su, K. Sun, "Properties of the frequency-amplitude curve," *IEEE Trans. Power Syst.*, vol. 32, no. 1, pp. 826-827, Jan. 2017.
- [19] B. Wang, K. Sun, W. Kang, "Nonlinear modal decoupling of multi-oscillator systems with applications to power systems," *IEEE Access*, vol. 6, pp. 9201-9217, 2018.
- [20] B. Wang, K. Sun, X. Xu, "Nonlinear modal decoupling based power system transient stability analysis," *IEEE Trans. Power Syst.*, vol. 34, no. 6, pp. 4889-4899, Jun. 2019.
- [21] J. Qi, K. Sun, J. Wang, H. Liu, "Dynamic state estimation for multimachine power system by unscented Kalman filter with enhanced numerical stability," *IEEE Trans. Smart Grid*, vol. 9, no. 2, pp. 1184-1196, Mar. 2018.
- [22] K. Sun, J. Qi, W. Kang, "Power System Observability and Dynamic State Estimation for Stability Monitoring Using Synchrophasor Measurements," *Control Engineering Practice*, vol. 53, pp. 160-172, August 2016
- [23] E. Ghahremani, I. Kamwa, "Online state estimation of a synchronous generator using unscented Kalman filter from phasor measurements units," *IEEE Trans. Energy Convers.*, vol. 26, no. 4, pp. 1099-1108, Dec. 2011.
- [24] F. Milano, A. Ortega, "Frequency divider," *IEEE Trans. Power Syst.*, vol. 32, no. 2, pp. 1493-1501, Mar. 2017.
- [25] J. Hox, M. Moerbeek, R. Van de Schoot, *Multilevel analysis: techniques and applications*, Routledge, 2017.
- [26] D. Eberly, "Derivative approximation by finite differences," *Magic Software, Inc*, 2008.
- [27] W. Ju, B. Wang, K. Sun, "Estimating transient stability margin regarding a dominant oscillation mode," *IEEE PES Powertech*, Milano, Italy, Jun. 2019.
- [28] R. Leelaruij, L. Vanfretti, K. Uhlen, J.O. Gjerde, "Computing sensitivities from synchrophasor data for voltage stability monitoring and visualization," *Int. J. Electr. Energy Syst.*, vol. 25, no. 6, pp. 933-947, Jun. 2015.
- [29] S. W. Smith. *The Scientist and Engineer's Guide to Digital Signal Processing*, California Technical Pub, 1997.
- [30] R. E. Blake, "Basic Vibration Theory," in *Shock and Vibration Handbook*. New York, NY, USA: McGraw Hill, 1988.
- [31] N. Zhou, J. W. Pierre, J. F. Hauer, "Initial results in power system identification from injected probing signals using a subspace method," *IEEE Trans. Power Syst.*, vol. 21, no. 4, pp. 1296-1302, Nov. 2006.
- [32] J. Chow, G. Rogers, User manual for power system toolbox, version 3.0, 1991-2008.
- [33] H. D. Chiang, *Direct Methods for Stability Analysis of Electric Power Systems: Theoretical Foundation, BCU Methodologies, and Applications*. Hoboken, NJ, USA: Wiley, 2011.
- [34] H. D. Chiang, F. Wu, P. Varaiya, "Foundations of direct methods for power transient stability analysis," *IEEE Trans. Circuits Syst.*, vol. 34, no. 2, pp. 160-173, Feb. 1987.
- [35] J. Qi, K. Sun, W. Kang, "Optimal PMU placement for power system dynamic state estimation by using empirical observability Gramian," *IEEE Trans. Power Syst.*, vol. 30, no. 4, pp. 2041-2054, Jul. 2015.
- [36] North American Electric Reliability Council and Federal Energy Regulatory Commission, Arizona—Southern California outages on September 8, 2011: Causes and recommendations. [Online]. Available: https://www.nerc.com/pa/rm/ea/September_2011_Southwest_Blackout_Event_Document/L/AZO outage_Report_01MAY12.pdf.



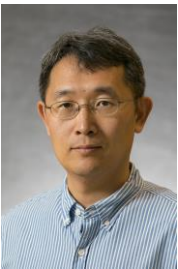
Xin Xu (S'15) received the Ph.D. degree in electrical engineering from University of Tennessee in 2020. Before that he received the B.E. and M.E. degree in electrical engineering from Shandong University, in 2013 and 2016, respectively. He is now an engineer in electric transmission operations engineering with Dominion Energy. His main research interests include data analytics in power systems, and nonlinear system dynamics, stability assessment and control.



Wenyun Ju (S'14-M'18) received the B.Sc. degree in electrical engineering and automation from Sichuan University, Chengdu, China in 2010, and the M.Sc. degree in electrical and electronic engineering from Huazhong University of Science and Technology, Wuhan, China in 2013, and his Ph.D. degree in electrical engineering from the University of Tennessee, Knoxville, TN, USA in 2018. He is currently a Power System Engineer with Electric Power Group, Pasadena, CA, USA.



Bin Wang (S'14-M'18) received the B.S. and M.S. degrees from Xi'an Jiaotong University, in 2011 and 2013, respectively, and the Ph.D. degree from the University of Tennessee in 2017, all in electrical engineering. He joined the Department of Electrical and Computer Engineering at Texas A&M University in 2018 as a postdoc. He is currently a postdoc with the Power Systems Engineering Center at National Renewable Energy Laboratory. His research interests include power system dynamics, stability and control.



Kai Sun (M'06–SM'13) received the B.S. degree in automation in 1999 and the Ph.D. degree in control science and engineering in 2004 both from Tsinghua University, Beijing, China. He is an associate professor at the Department of EECS, University of Tennessee, Knoxville, USA. He was a project manager in grid operations and planning at the EPRI, Palo Alto, CA from 2007 to 2012. Dr. Sun serves in the editorial boards of IEEE Transactions on Power Systems, IEEE Transactions on Smart Grid, IEEE Access and IEEE Open Access Journal of Power and Energy.